Physica Scripta

PAPER

Ab initio investigation of structural, elastic, and thermodynamic characteristics of tetragonal XAgO compounds (X = Li, Na, K, Rb)

RECEIVED
26 April 2023

REVISED
8 September 2023

ACCEPTED FOR PUBLICATION
21 September 2023

PUBLISHED
4 October 2023

Djamel Allali[1,2,*], **Rabie Amari**[3,4], **Abdelmadjid Bouhemadou**[5], **Ammar Boukhari**[4,6], **Bahri Deghfel**[7], **Saber Saad Essaoud**[8], **Saad Bin-Omran**[9], **Missoum Radjai**[10], **Rabah Khenata**[11] and **Yarub Al-Douri**[12,13,14]

[1] Physics and Chemistry of Materials Lab, Department of Physics, University of M'sila, 28000, M'sila, Algeria
[2] University of M'sila, Faculty of Technology, B.P. 166 Ichbilia, 28000, M'sila, Algeria
[3] Department of Civil Engineering, Faculty of Technology, University of M'sila, Algeria
[4] Laboratory of Materials and Renewable Energy, Faculty of Sciences, Mohamed Boudiaf University of M'sila, 28000, M'sila, Algeria
[5] Laboratory for Developing New Materials and their Characterizations, Department of Physics, Faculty of Sciences, Ferhat Abbas University - Setif 1, 19000 Setif, Algeria
[6] Department of Mechanical Engineering, Faculty of Technology, University of M'sila, Algeria
[7] University of M'sila, Faculty of Science, Department of Physics, 28000, M'sila, Algeria
[8] Department of Physics, Faculty of Science, University of M'sila, 28000, M'sila, Algeria
[9] Department of Physics and Astronomy, College of Science, King Saud University, PO Box 2455, Riyadh 11451, Saudi Arabia
[10] Laboratory of Physics of Experimental Techniques and Their Applications University of Medea, 26000 Medea, Algeria
[11] Laboratoire de Physique Quantique de la Matière et de Modélisation Mathématique (LPQ3M), Université de Mascara, 29000 Mascara, Algeria
[12] Department of Applied Physics and Astronomy, College of Sciences, University of Sharjah, PO Box 27272, Sharjah, United Arab Emirates
[13] Department of Mechanical Engineering, Faculty of Engineering, Piri Reis University, EflatunSk. No:8, 34940 Tuzla, Istanbul, Turkey
[14] Nanotechnology and Catalysis Research Centre, University of Malaya, 50603 Kuala Lumpur, Malaysia
[*] Author to whom any correspondence should be addressed.

E-mail: djamel.allali@univ-msila.dz

Keywords: Ag-based oxides, *Ab initio* calculations, structural parameters, elastic moduli, thermal properties

Abstract

The present research utilizes *ab initio* computations to examine the thermodynamic, structural, and elastic characteristics of XAgO ternary oxides, where X signifies Li, Na, K, and Rb.The GGA-PBE and GGA-WC functionals were used to calculate the ground-state lattice parameters and atomic position coordinates of the title materials. The calculated results were in good agreement with both experimental measurements and theoretical predictions. This suggests that the GGA-PBE and GGA-WC functionals are accurate for describing the structural properties of the material under study.This study offers computational predictions for the elastic properties of monocrystalline structures and polycrystalline aggregates of XAgO compounds. These predictions encompass various key parameters, including single-crystal elastic constants, Young's modulus, bulk modulus, Lame coefficients, Poisson's ratio, shear modulus, and Debye temperature. Additionally, the quasi-harmonic Debye approximation is utilized to explore the temperature-dependent behavior of bulk modulus, Debye temperature, volume thermal expansion coefficient, and isobaric and isochoric heat capacities over an extensive temperature range, while maintaining constant pressures. The results obtained from this model are found to be highly successful in accurately predicting the behavior of these properties.

1. Introduction

Noncentrosymmetric oxides are a group of materials that have attracted considerable interest owing to their properties, which are dependent on their symmetry, such as ferroelectricity, piezoelectricity, pyroelectricity, and nonlinear optical (NLO) characteristics. These properties make the noncentrosymmetric oxides highly promising for a wide range of applications, such as ferroelectricity,second-order nonlinear optical, actuators and sensors [1–4]. Among the noncentrosymmetric oxides, the XAgO [X: Li, Na, K, Rb] materials, which are the focus of the present study, are classified as non-polar noncentrosymmetric systems and are known to crystallize

in the tetragonal KAgO-type structure under ambient conditions [4–7]. Some previous studies have reported data on the synthesis and structural features of XAgO [X: Li, Na, K, Rb] compounds [5–7]. The tetragonal crystal structure of XAgO materials has been determined through the analysis of X-ray diffraction spectra obtained from single crystals [4–6]. Umamaheswari *et al* [4] investigated the electronic and structural properties of NaAgO, KAgO, and RbAgO compounds using the tight-binding linear muffin-tin orbital (TB-LMTO) method with local density approximation (LDA).

Although experimental and theoretical studies have been conducted on the XAgO (X = Li, Na, K, Rb) materials [4–7], it is important to note that certain fundamental physical properties of these materials remain incompletely investigated and scarcely reported in the literature. As a result, there is a significant knowledge gap in understanding the full range of their intrinsic properties, which has implications for their potential practical applications. Given the limited and scarce information currently available, it is essential to conduct further in-depth investigations into the fundamental physical properties of these materials. These additional studies are critical for bridging the existing knowledge gaps and gaining a comprehensive understanding of the materials intrinsic properties. By exploring the unexplored aspects, researchers can gain valuable insights into the materials' behavior, responses to external stimuli, and potential applications. As a result, this expanded knowledge will pave the way for fully utilizing the potential of these materials in future applications.

In the context of integrating semiconductor materials into various technological applications, it is essential to have a comprehensive understanding of their fundamental physical properties. Two key properties, namely elastic and thermodynamic properties, play a central role in this field. Semiconductor materials are commonly fabricated in the form of thin films on substrates. This growth method introduces a mismatch between the lattice parametersof the thin films and the underlying substrates. As a result, the thin films are subjected to stress, which can significantly impact their physical properties. Therefore, it is important to understand the elastic properties of these materials and how pressure influences their structural and elastic characteristics. This knowledge can be used to effectively engineer and optimize the performance of semiconductor materials for practical applications. Furthermore, semiconductor materials are often used in optoelectronic devices, which typically operate at relatively elevated temperatures. In this context, it is essential to investigate and understand the effects of temperature variations on the macroscopic physical parameters of these materials. Gaining insight into the temperature-dependent behavior of semiconductor materials is crucial for ensuring the stability, reliability, and efficient functioning of optoelectronic devices under real-world operating conditions. By exploring the interplay between temperature and material properties, researchers can devise strategies to enhance the thermal performance and overall reliability of optoelectronic technologies. However, the thermal and elastic properties of XAgO [X: Li, Na, K, Rb] materials have not been studied either theoretically or experimentally, despite their critical role in understanding the fundamental physical characteristics of materials and their behavior under external constraints like high pressure and temperature.

Measuring the single-crystal elastic constants and effects of temperature and pressure on physical parameters can be challenging, making theoretical calculations a reliable alternative. *Ab initio* methods are particularly useful in predicting the physical properties of materials that have not yet been experimentally studied [8, 9]. In this study, we employ the density functional theory (DFT) based pseudopotential plane-wave (PP-PW) method to forecast the pressure dependence of the structural and elastic properties of LiAgO, NaAgO, KAgO, and RbAgO compounds. Furthermore, we combine the PP-PW method with the quasi-harmonic Debye approximation to successfully predict the temperature and pressure-dependent behavior of the thermodynamic properties of the considered compounds. The outcomes of this study enhance the understanding of the essential properties of XAgO materials and their potential for practical applications.

2. Description of computational techniques and parameters

The computations were carried out using the pseudopotential planewave method (PP-PW) as implemented in the CASTEP software [10]. It is noteworthy to acknowledge that the PP-PW method represents the cutting-edge approach for the geometrical optimization of crystals. In this study, we incorporated two distinct versions of the generalized gradient approximation (GGA) to model the exchange–correlation interactions during the geometry optimization process. Specifically, the GGA-PBEsol [11] and GGA-WC [12] functionals were employed for this purpose. However, when studying other properties of the studied crystals, we only used the functional GGA-PBEsol. The rationale for this decision stems from the fact that the GGA-PBEsol and the GGA-WC reproduce nearly identical values for the structural parameters. To model the potential generated by the nucleus and frozen electrons, an ultra-soft Vanderbilt-type pseudopotential [13] was utilized and applied to the valence electrons. The valence electrons of Li ($1s^2 2s^1$, O ($2s^2 2p^4$), Ag($4d^{10} 5s^1$), K($3s^2 3p^6 4s^1$), Na($2s^2 2p^6 3s^1$) and Rb ($4s^2 4p^6 5s^1$) were taken into account. The plane-wave basis set, which expands the electron wave functions, was truncated at maximum plane-wave energy (E_{cut}) of 400 eV. The Brillouin zone was sampled using a

6 × 6 × 3 Monkhorst-Park special k-mesh [14].It is important to note that the selection of these computational parameters was based on thorough convergence tests of the total energy.

The optimized crystal geometry was acquired using the Broyden–Fletcher–Goldfarb–Shanno (BFGS) minimization technique for geometries [15]. The convergence criteria for energy change, maximal stress, maximal force, and maximal displacement were set to 5×10^{-7} eV atom^{-1}, 0.02 GPa, 0.01 eV Å, and 5.0×10^{-4}Å, respectively. Electronic occupation was smoothed using the Gaussian scheme, with a smearing width of 0.1 eV. The monocrystalline elastic constants (C_{ij}) were determined using the finite strain-stress method, and the polycrystalline elastic moduli were derived using the Voigt-Reuss-Hill approximation [16–20].

As a general rule, *ab initio* calculations are performed at T = 0 K, where no thermal excitation of the nuclei is considered. To account for this effect without relying on empirical values, two approaches are generally used: the quasi-harmonic Debye model coupled with an *ab initio* calculation, or the phonon dispersion relations. In this study, the quasi-harmonic Debye approximation implemented in the GIBBS code [21] in combination with the PP-PW method was used.

3. Findings and analysis

3.1. Characteristics of the crystal structure

The tetragonal noncentrosymmetric materials XAgO (X = Li, Na, K and Rb), which have a space group of *I4/mmm* (no.139), contain two chemical formula units in their unit cell (Z = 2). The positions of the Ag, O, and alkaline metal X atoms are located at 8 h (x_{Ag}, x_{Ag}, 0), 8i (x_O, 0, 0), and 8j (0.5, y_X, 0), respectively, where x_{Ag}, x_O, and y_X are the internal coordinates of the corresponding atoms. The symmetry group does not fix five structural parameters, which consist of the two lattice parameters ('*a*' and '*c*') and the three internal coordinates (x_{Ag}, x_O, and y_X). In table 1, we provide the calculated ground state structural parameters for XAgO materials using the GGA-PBEsol, and GGA-WC functionalsalong with existing theoretical and experimental data for comparison. The calculated ground-state structural parameters, in particular the volume of the conventional unit cell, show that the GGA-PBEsol and GGA-WC functionals yield nearly identical results. The differences between the results obtained using these two exchange–correlation functionals are negligible. Our results, including the obtained lattice parameters ('*a*' and '*c*'), and internal parameters (x_{Ag}, x_O, and y_X) at zero pressure, are in good agreement with available experimental data. The maximal deviation of '*a*' and '*c*' from the corresponding experimental values are less than 1.5%, indicating the accuracy and reliability of the results of our calculations. The calculated values of the internal coordinates, namely x_{Ag}, x_O, and y_X, also exhibit substantial agreement with their corresponding experimental counterparts. The trend of '*a*' and '*c*' values of XAgO materials follows the order of $\{a;\ c\}(LiAgO) < \{a;\ c\}(NaAgO) < \{a;\ c\}(KAgO) < \{a;\ c\}(RbAgO)$, which can be explained by comparing the atomic radii (R) of X atoms in the same column of the periodic table (R(Rb) = 2.98Å, R(K) = 2.77Å, R(Na) = 2.23Å, and R(Li) = 2.05Å). Specifically, the larger the atomic radius of X (X: Li, Na, K, Rb), the larger the lattice parameters.

In order to check the structural and thermodynamic stabilities of XAgO ternary oxides, where X signifies Li, Na, K, and Rb, we have calculated their formation enthalpies (ΔH) and cohesive energies (E_{coh}) using the following expressions [22]:

$$\Delta H = \frac{1}{n_X + n_{Ag} + n_O} \times [E_{tot}^{XAgO} - (n_X E_{tot}^{X(Solid)} + n_{Ag} E_{tot}^{Ag(Solid)} + n_O E_{tot}^{O(Solid)})];$$

$$E_{coh} = \frac{1}{n_X + n_{Ag} + n_O} \times [E_{tot}^{XAgO} - (n_X E_{tot}^{X(atom)} + n_{Ag} E_{tot}^{Ag(atom)} + n_O E_{tot}^{O(atom)})].$$

Here, the total energy of the primitive cell of XAgO is represented by E_{tot}^{XAgO}, the total energies per atom of the solid state of the pure X (X = Li, Na, K, Rb), Ag and O elements are represented by $E_{tot}^{X(Solid)}$, $E_{tot}^{Ag(Solid)}$ and $E_{tot}^{O(atom)}$, respectively, $E_{tot}^{X(atom)}$, $E_{tot}^{Ag(atom)}$ and $E_{tot}^{O(atom)}$ represent the total energies of the isolated X, Ag, and O atoms, and n_X, n_{Ag} and n_O represent the number of X, Ag, and O atoms in the primitive cell. The calculated values of the formation enthalpies and cohesive energies for XAgO (X = Li, Na, K, Rb) are shown in table 1. It is found that all considered compounds have negative formation enthalpies and cohesive energies, highlighting their structural and energetic stabilities in the tetragonal structure. Furthermore, as depicted in figure 1, the investigated crystalline substances exhibit a conspicuous characteristic wherein their respective formation enthalpies exhibit negativity across distinct pressure intervals that coincide with their mechanical stability thresholds. Specifically, this trend is manifest within the pressure ranges of 0 to 14 GPa for LiAgO, 0 to 12 GPa for NaAgO, 0 to 8 GPa for KAgO, and 0 to 6 GPa for RbAgO. These results confirm the remarkable flexibility of LiAgO, NaAgO, KAgO, and RbAgO, as they demonstrate long-lasting structural integrity when subjected to stress conditions consistent with the inherent limits of structural stability.

Table 1. The computed ground-state equilibrium lattice parameters (*'a'* and *'c'*, in Å), volume (V, in Å^3), bond lengths (Ag–O and X–O, in Å), internal coordinates (y_X, x_{Ag}, and x_O), bulk modulus (B, in GPa), first pressure derivative of the bulk modulus (B'), the formation enthalpies (ΔH, in eV/atom) and the cohesive energy (E_{coh}, in eV/atom), for the Ag-based ternary oxides: LiAgO, NaAgO, KAgO, and RbAgO. Experimental values are also included for comparison. The bulk modulus and its first pressure derivative were obtained from the Birch equation of state P(V).

Parameter	Materials							
	LiAgO		NaAgO		KAgO		RbAgO	
	Present	Expt.	Present	Expt.	Present	Expt.	Present	Expt.
a	9.176[a]	9.248[d]	9.429[a]	9.522[d]	9.777[a]	9.893[d,e]	10.01[a]	10.089[d]
	9.189[b]		9.447[b]	9.520[e,f]	9.798[b]	9.925[f]	10.027[b]	10.086[e]
			9.670[c]		10.08[c]		10.35[c]	10.02[f]
c	3.816[a]	3.75[d]	4.655[a]	4.602[d]	5.390[a]	5.445[d,e]	5.788[a]	5.796[d]
	3.819[b]		4.643[b]	4.599[e]	5.373[b]	5.458[f]	5.752[b]	5.792[e]
			4.699[c]	4.617[f]	5.614[c]		6.034[c]	5.67[f]
V	321.30[a]	320.72[d]	413.85[a]	416.98[d]	515.23[a]	532.91[d]	579.95[a]	589.96[d]
	322.46[b]		414.36[b]		515.81[b]		578.31[b]	
c/*a*	0.4158[a]		0.493[a]	0.483[e]	0.551[a]	0.55[e,f]	0.578[a]	0.574[e]
	0.4156[b]		0.491[b]	0.49[f]	0.548[b]		0.573[b]	0.57[f]
			0.486[c]		0.557[c]		0.583[c]	
y_X	0.138[a]		0.161[a]	0.159[f]	0.176[a]	0.1772[f]	0.184[a]	0.1837[f]
	0.138[b]		0.162[b]		0.176[b]		0.184[b]	
x_{Ag}	0.162[a]		0.158[a]	0.155[f]	0.149[a]		0.145[a]	0.1457[f]
	0.162[b]		0.158[b]		0.149[b]	0.1478[f]	0.145[b]	
x_O	0.322[a]		0.310[a]	0.306[f]	0.298[a]		0.291[a]	0.2893[f]
	0.322[b]		0.310[b]		0.298[b]	0.2944	0.291[b]	
B	71.34[a]		47.18[a]		32.41[a]		28.19[a]	
	69.86[b]		46.11[b]		31.23[b]		26.50[b]	
			64[c]		41[c]		33[c]	
B'	4.79[a]		5.28[a]		5.03[a]		5.27[a]	
	4.77[b]		5.30[b]		**5.112**[b]		6.66[b]	
d(Ag-O)	2.093[a]		2.073[a]		**2.065**[a]		2.064[a]	
d(X-O)	2.066[a]		2.350[a]		**2.619**[a]		2.791[a]	
ΔH	-1.578[a]		-1.354[a]		**-1.384**[a]		-1.329[a]	
E_{coh}	-4.557[a]		-4.276[a]		**-4.093**[a]		-3.995[a]	

[a] Present work using the GGA-PBEsol
[b] Present work using the GGA-WC
[c] [4],
[d] [5],
[e] [6],
[f] [7].

In order to study the influence of the external pressure on the structural properties of XAgO (X = Li, Na, K, and Rb), we analyzed the variations of the lattice parameters '*a*' and '*c*' as a function of pressure in pressure intervals that coincide with their mechanical stability thresholds, namely in the pressure ranges of 0 to 14 GPa for LiAgO, 0 to 12 GPa for NaAgO, 0 to 8 GPa for KAgO and 0 to 6 GPa for RbAgO.At each pressure step, a complete structural optimization was carried out. The relative variation in the lattice parameters was depicted as a plot of a/a_0 and c/c_0 against the external hydrostatic pressure P, where *a* and *c* denote the values of the lattice parameters at a given pressure P, and a_0 and c_0 represent the corresponding values at zero pressure. This information is presented in figure 2. The symbols in the plot illustrate the outcomes of the *ab initio* calculations for the specific pressures, while the solid lines demonstrate the results fitness to a quadratic polynomial form, expressed as $A/A_0 = 1 + \alpha P + \beta P^2$, where *A* is the lattice parameter value at the P pressure and A_0 is the lattice parameter value at zero pressure. The obtained results for the materials under consideration are as follows:

$$\text{LiAgO}\begin{cases}\dfrac{a}{a_0} = 1 - 0.0032P + 4.10097 \times 10^{-5}P^2 \\ \dfrac{c}{c_0} = 1 - 0.00681P + 15.5198 \times 10^{-5}P^2\end{cases}$$

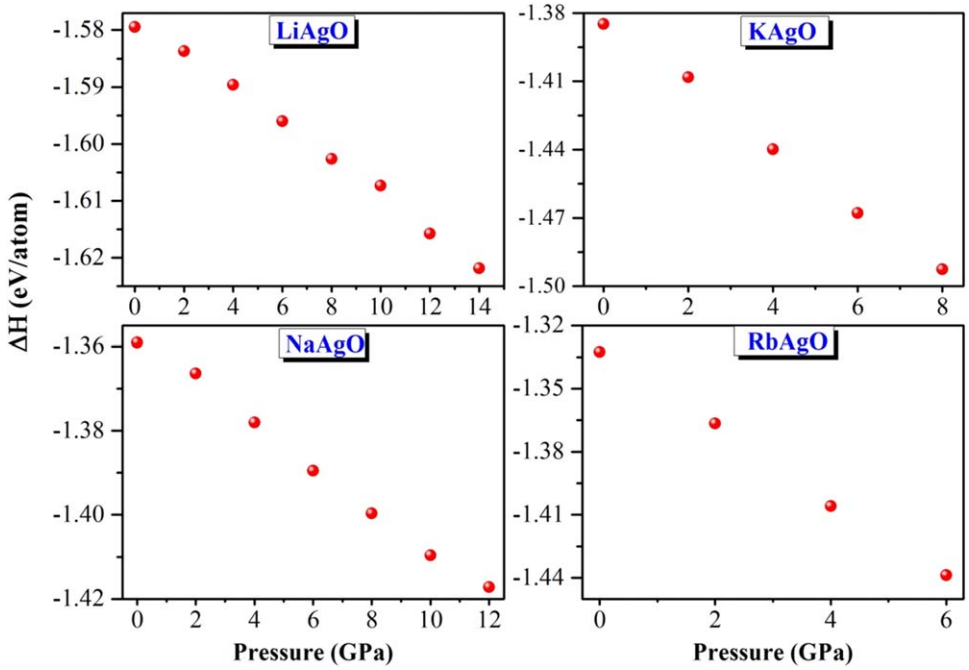

Figure 1. Pressure dependence of the formation enthalpies (ΔH) for XAgO (X = Li, Na, K, Rb).

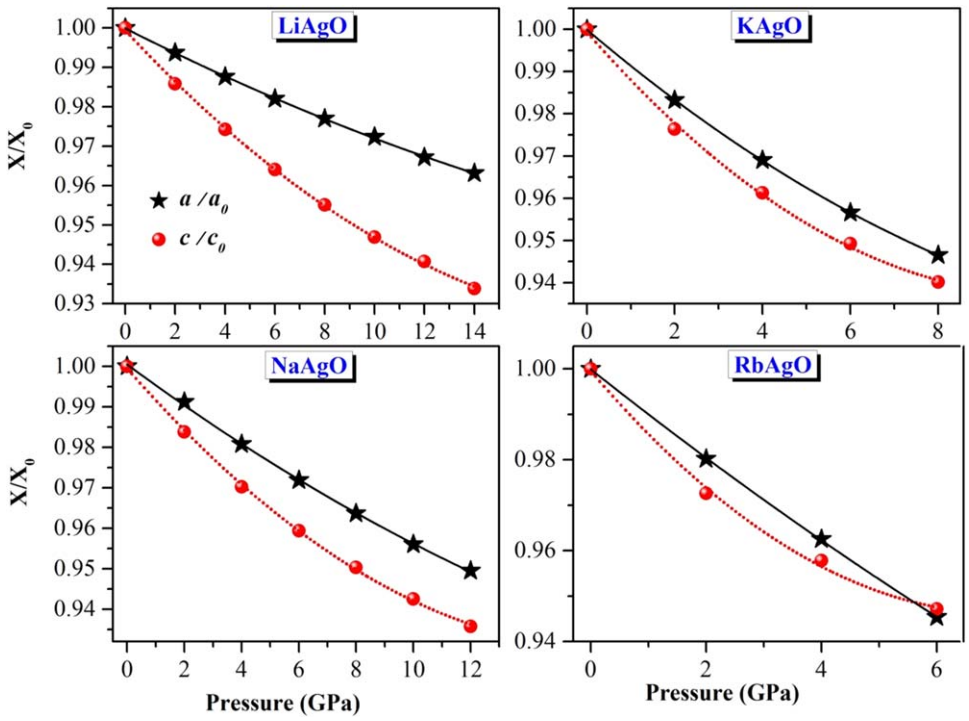

Figure 2. Pressure dependence of the relative changes in the lattice constants '*a*' and '*c*' for the materials LiAgO, NaAgO, KAgO, and RbAgO. The subscript '0' indicates the lattice parameter value at zero pressure.

$$\text{NaAgO}\begin{cases}\dfrac{a}{a_0} = 1 - 0.00521P + 7.88737 \times 10^{-5}P^2 \\ \dfrac{c}{c_0} = 1 - 0.00811P + 23.7189 \times 10^{-5}P^2\end{cases}$$

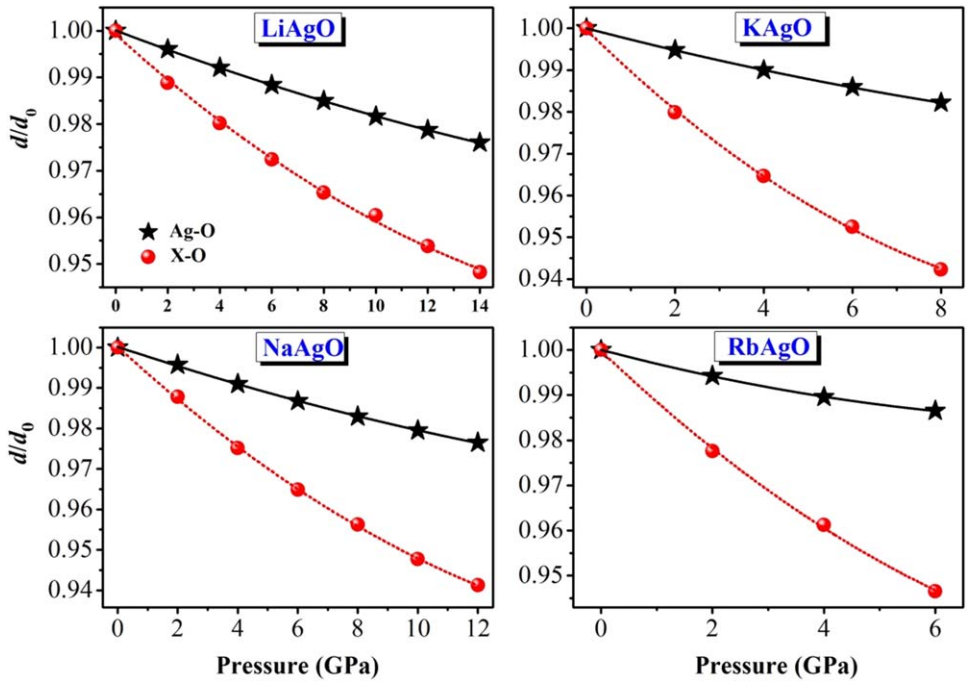

Figure 3. Pressure-dependent variations in the relative bond lengths for the compounds LiAgO, NaAgO, KAgO, and RbAgO. The calculated values for these compounds are represented by symbols, while the quadratic approximations are depicted using solid lines. In this context, 'd' denotes the interatomic distance at a given pressure P, and 'd_0' signifies the same distance under zero pressure.

$$\text{KAgO}\begin{cases}\dfrac{a}{a_0} = 1 - 0.00884P + 27.0292 \times 10^{-5}P^2 \\ \dfrac{c}{c_0} = 1 - 0.01192P + 57.2327 \times 10^{-5}P^2\end{cases}$$

$$\text{RbAgO}\begin{cases}\dfrac{a}{a_0} = 1 - 0.01006P + 16.4051 \times 10^{-5}P^2 \\ \dfrac{c}{c_0} = 1 - 0.01494P + 105 \times 10^{-5}P^2\end{cases}$$

The study investigated the shrinkage degree and stiffness of LiAgO, NaAgO, KAgO, and RbAgO when subjected to unidirectional stress along the 'a' and 'c' directions. Results showed that the shrinkage degree (linear compressibility) along the 'a' and 'c' directions increases as the atomic number Z of the X atom (Li, Na, K, and Rb) increases from LiAgO to RbAgO. Furthermore, it is evident that within the crystalline compounds LiAgO, NaAgO, and KAgO, the linear compressibility along the c-axis surpasses that along the a-axis. In the case of RbAgO, a distinct behavior is observed. Up to a pressure threshold of 5.6 GPa, the linear compressibility along the c-axis remains superior to that along the a-axis. However, beyond this point, a reversal occurs, and the linear compressibility along the a-axis overtakes that along the c-axis. These findings suggest that LiAgO, NaAgO and KAgO are more resistant to unidirectional stress applied along the a-axis than along the c-axis, while RbAgO shows similar behavior up to 5.6 GPa.

In our investigation, we scrutinized the proportional fluctuations in bond lengths involving Ag-O and X-O (where X represents Li, Na, K, and Rb) within XAgO materials under varying pressure conditions. These analyses were conducted within pressure intervals that align precisely with the designated thresholds of mechanical stability for the respective materials. To be specific, these pressure intervals span from 0 to 14 GPa for LiAgO, 0 to 12 GPa for NaAgO, 0 to 8 GPa for KAgO, and 0 to 6 GPa for RbAgO, as visually illustrated in figure 3. The findings show that the Ag-O chemical bond was the stiffest, while the X-O bond is the weakest in all the studied materials. Additionally, the replacement of Li with Na, Na with K, and K with Rb led to a further weakening of the X-O bond, which may explain the observed shrinkage along the a-axis in these materials. The elongation observed in the X-O bond length, when substituting Li with Na, Na with K, and K with Rb in the XAgO compounds (where X represents Li, Na, K, or Rb), can be attributed to the gradual increase in the atomic radii of the respective X atoms within the sequence. This phenomenon elucidates the diminished strength of the X-O bond, as observed in the progression from LiAgO to NaAgO to KAgO to RbAgO. We used quadratic least-squares fit equations ($d/d_0 = 1 + \alpha P + \beta P^2$) to approximate the relative variations of the Ag-O and X-O bond lengths under pressure. The Ag-O and X-O bond lengths at any pressure up to 14 GPa can estimated using the

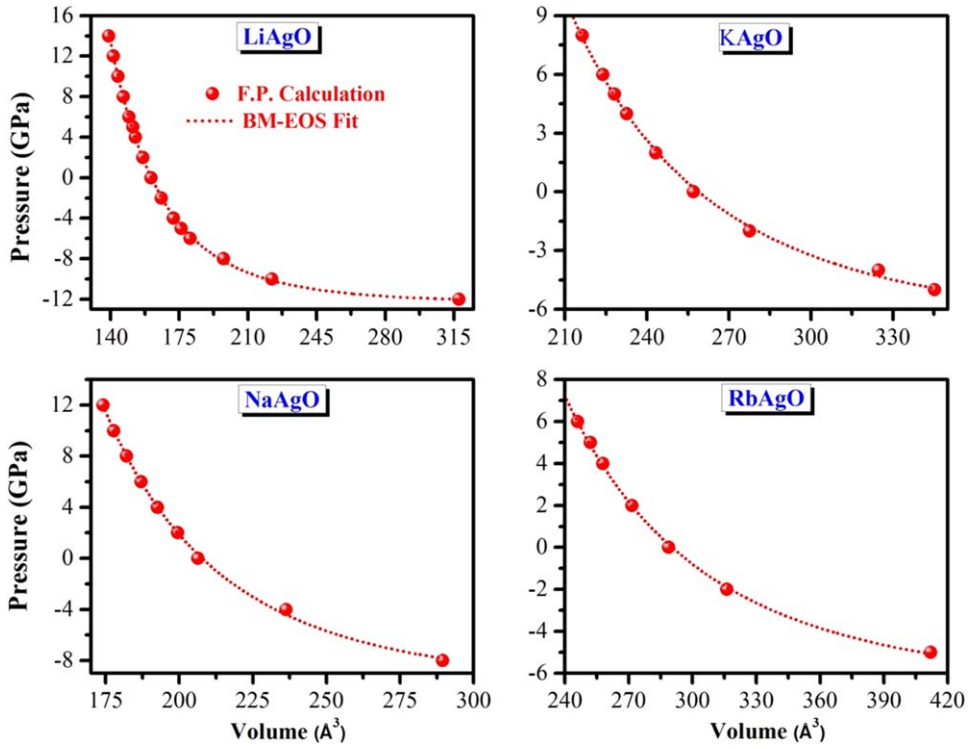

Figure 4. Pressure dependence of the primitive-cell volume for LiAgO, NaAgO, KAgO, and RbAgO. The symbols represent the *ab initio* calculated P-V data, while the continuous lines indicate the fits of the P-V data to the Birch-Murnaghan equation of state.

following expressions:

$$\text{LiAgO}\begin{cases} Ag-O: \dfrac{d}{d_0} = 1 - 0.00212P + 2.8246 \times 10^{-5}P^2 \\ X-O: \dfrac{d}{d_0} = 1 - 0.00505P + 10.3788 \times 10^{-5}P^2 \end{cases}$$

$$\text{NaAgO}\begin{cases} Ag-O: \dfrac{d}{d_0} = 1 - 0.00247P + 4.09457 \times 10^{-5}P^2 \\ X-O: \dfrac{d}{d_0} = 1 - 0.00681P + 15.7487 \times 10^{-5}P^2 \end{cases}$$

$$\text{KAgO}\begin{cases} Ag-O: \dfrac{d}{d_0} = 1 - 0.00276P + 6.68389 \times 10^{-5}P^2 \\ X-O: \dfrac{d}{d_0} = 1 - 0.0104P + 40.8072 \times 10^{-5}P^2 \end{cases}$$

$$\text{RbAgO}\begin{cases} Ag-O: \dfrac{d}{d_0} = 1 - 0.00327P + 16.8615 \times 10^{-5}P^2 \\ X-O: \dfrac{d}{d_0} = 1 - 0.01175P + 48.5711 \times 10^{-5}P^2 \end{cases}$$

The equations provided above offer a means to approximate the Ag-O and X-O bond lengths at any given pressure value falling within the confines of the compounds mechanical stability threshold.

We utilized the pressure dependence of the primitive cell volume (as shown in figure 4) to construct the equation of state P(V). The bulk modulus at zero pressure (B) and its pressure derivative (B') are then estimated by fitting the P-V data to the third-order Birch-Murnaghan equation of state (EOS) [23, 24], which is represented by solid lines in figure 4 and tabulated in table 1. The obtained values of B for the title compounds, using the GGA-PBEsoland GGA-WC functionals, are found to be slightly smaller than those reported in a previous study [4]. This discrepancy may be attributed to the use of the LDA functional in [4], which is known to overestimate B compared to the one obtained by the GGA functional. Unfortunately, no experimental values for B and B' are available in the literature to confirm our results. Furthermore, the calculated B values for the title

Table 2. Computed elastic properties including elastic constants (C_{ij}, in GPa), bulk modulus (B, in GPa), shear modulus (G, in GPa), Pugh's ratio (B/G), Young's modulus (E, in GPa), Poisson's ratio (σ), Lamé's coefficient (λ, in GPa), longitudinal, transverse and average sound velocities (V_l, V_t and V_m, respectively, in m s^{-1}), and Debye temperature (θ_D, in K) for LiAgO, NaAgO, KAgO and RbAgO. The bulk modulus is determined from the C_{ij} values, while the C_{ij} values for isostructural compounds are provided for comparison.

Parameter	Materials							
	LiAgO	LiCuO	NaAgO	NaCuO	KAgO	KCuO	RbAgO	RbCuO
C_{11}	116.1	125.5[a]	82.9	86.4[a]	59.3	58.5[a]	50.0	48.3[a]
C_{33}	95.976	94.3[a]	76.4	73.8[a]	57.9	53.7[a]	52.4	47.6[a]
C_{44}	15.8	25.1[a]	13.6	15.4[a]	9.1	9.5[a]	7.2	7.0[a]
C_{66}	60.9	58.7[a]	34.6	34.7[a]	21.9	23.5[a]	17.3	19.3[a]
C_{12}	83.3	72.7[a]	51.0	41.8[a]	29.3	25.4[a]	23.6	21.3[a]
C_{13}	41.1	40.0[a]	21.7	21.3[a]	14.6	14.4[a]	13.6	13.9[a]
B_R	69.4		46.5		32.2		28.1	
B_V	73.2		47.9		32.6		28.2	
B_H	71.3		47.2		32.4		28.2	
G_R	21.6		18.5		13.4		10.8	
G_V	29.3		22.2		15.9		13.1	
G_H	25.5		20.4		14.6		12.0	
B_H/G_H	2.8		2.32		2.22		2.36	
E	68.2		53.4		38.1		31.4	
σ	0.341		0.311		0.304		0.314	
λ	53.7		33.1		52.0		19.5	
V_l	4418.4		3970.9		3514.7		3033.7	
V_t	2172.6		2077.9		1864.9		1579.1	
V_m	2439.6		2324.4		2084.2		1767.0	
θ_D	340.1		288.7		275.1		210.1	

[a] [25].

compounds exhibit a decreasing trend as follows: $B^{LiAgO} > B^{NaAgO} > B^{KAgO} > B^{RbAgO}$. This trend corresponds to an increase in unit cell volume V, which follows the sequence: $V^{LiAgO} < V^{NaAgO} < V^{KAgO} < V^{RbAgO}$. It is therefore evident that the bulk modulus (B) decreases with increasing unit cell volume (V), in accordance with the well-established relationship between B and V: $B \propto V^{-1}$.

3.2. Elasticity characteristics

3.2.1. Elastic constants of the monocrystalline phase

Accurate numerical estimation of elastic constants (C_{ij}) is crucial in predicting the physical properties of materials. Specifically, these constants play a crucial role in determining the mechanical stability, elasticity, and strength of crystals. In the case of tetragonal crystals, the six independent elastic constants that fully characterize their elastic properties are C_{11}, C_{33}, C_{44}, C_{66}, C_{12}, and C_{13}. Present computed values for the elastic constants of XAgO (X = Li, Na, K, and Rb) oxides are listed in table 2. Note that there are no experimental or previously calculated values for C_{ij}s available in the literature for comparison [25]. In table 2, we also provide the elastic constants of is structural LiCuO, NaCuO, KCuO, and RbCuO compounds to facilitate comparisons. The results reveal that C_{11} and C_{33}, representing the crystals resistance to unidirectional compression along the [100]/[010] and [001] crystallographic directions, respectively, are greater than C_{44}, C_{66}, C_{12}, and C_{13}, representing the crystals resistance to shear deformations. This suggests that the title compounds exhibit higher resistance to unidirectional compression than to shear strains. Furthermore, in LiAgO, NaAgO, and KAgO, C_{11} is greater than C_{33}, implying that the compounds have higher resistance to unidirectional stress along the [100]/[010] direction than along the [001] direction. This result is consistent with the hydrostatic pressure dependence of the lattice parameters '*a*' and '*c*' (section 3.1). Moreover, all calculated C_{ij}s of the title compounds satisfy the mechanical stability criteria for tetragonal crystals [26]: $C_{11} \succ 0$; $C_{33} \succ 0$; $C_{44} \succ 0$; $C_{66} \succ 0$; $C_{11} + C_{33} - 2C_{13} \succ 0$; $C_{11} - C_{12} \succ 0$; $2(C_{11} + C_{12}) + 4C_{13} + C_{33} \succ 0$, highlighting the mechanical stabilityof these materials.

By utilizing the computed monocrystalline elastic constants (C_{ij}s), it is possible to determine the linear compressibility along the *a* and *c* axes, referred to as β_a and β_c, respectively. These values can be obtained through the utilization of the following equations [27]:

$$\beta_a = \beta_b = (C_{33} - C_{13})/(C_{33}(C_{11} + C_{12}) - 2C_{13}^2) \quad (1)$$

$$\beta_c = (C_{11} + C_{12} - 2C_{13})/(C_{33}(C_{11} + C_{12}) - 2C_{13}^2) \quad (2)$$

The obtained β_a and $\beta_c$values for LiAgO, NaAgO, KAgO and RbAgO are:

$$\beta_a^{LiAgO} = 34.8 \times 10^{-4} GPa^{-1};\ \beta_c^{LiAgO} = 74.4 \times 10^{-4} GPa^{-1}$$
$$\beta_a^{NaAgO} = 58.9 \times 10^{-4} GPa^{-1};\ \beta_c^{NaAgO} = 97.4 \times 10^{-4} GPa^{-1}$$
$$\beta_a^{KAgO} = 92.1 \times 10^{-4} GPa^{-1};\ \beta_c^{KAgO} = 126.3 \times 10^{-4} GPa^{-1}$$
$$\beta_a^{RbAgO} = 111.2 \times 10^{-4} GPa^{-1};\ \beta_c^{RbAgO} = 133.0 \times 10^{-4} GPa^{-1}$$

From the linear compressibility β_a and β_c, it is possible tocalculate the volume compressibility β using the following relation: $\beta = 2\beta_a + \beta_c$. The obtained values for β are: $\beta^{\mathrm{LiAgO}} = 144.0 \times 10^{-4}\mathrm{GPa}^{-1}$; $\beta^{\mathrm{NaAgO}} = 215.0 \times 10^{-4}\mathrm{GPa}^{-1}$; $\beta^{\mathrm{KAgO}} = 310.0 \times 10^{-4}\mathrm{GPa}^{-1}$; $\beta^{\mathrm{RbAgO}} = 355.4 \times 10^{-4}\mathrm{GPa}^{-1}$. The estimated bulk modulus values from the well-known relation $B = 1/\beta$ are: $B^{\mathrm{LiAgO}} = 69.4\mathrm{GPa}$; $B^{\mathrm{NaAgO}} = 46.5\mathrm{GPa}$; $B^{\mathrm{KAgO}} = 32.3\mathrm{GPa}$; $B^{\mathrm{LiAgO}} = 28.1\mathrm{GPa}$. These B values are very close to those obtained from fitting the P(V) curves to the Birch equation of state and from analyzing the pressure dependence of the lattice parameters a and c(section 3.1). These findings serve to validate the accuracy of the outcomes pertaining to both the elastic constants and the pressure-induced variations in the structural parameters.

3.2.2. Elastic anisotropy

The assessment of the degree of elastic anisotropy in crystals is of significant interest due to its implications in physical phenomena such as the induction of microcracks [28]. Various metrics have been developed to investigate the extent of elastic anisotropy in crystals [29]. A common approach for characterizing the degree of elastic anisotropy in crystals is through three-dimensional (3D) visualization of the crystal direction dependence of elastic moduli, including linear compressibility and Young's modulus. The crystal direction dependence of the linear compressibility (β) and Young's modulus (E) in a tetragonal system can be expressed as follows [30]:

$$\begin{cases} \dfrac{1}{E} = (l_1^4 + l_2^4)S_{11} + l_3^4 S_{33} + 2l_1^2 l_2^2 S_{12} + 2(l_1^2 l_3^2 + 2l_2^2 l_3^2)S_{13} + (l_2^2 l_3^2 + l_1^2 l_3^2)S_{44} + l_1^2 l_2^2 S_{66} \\ \beta = (S_{11} + S_{12} + S_{13}) - (S_{11} + S_{12} - S_{13} - S_{33})l_3^2 \end{cases}$$

It should be noted that the representation of the crystal direction dependence of an elastic modulus in 3D takes the form of a closed surface. The distance between the center of the surface and any point on it in a given direction corresponds to the amplitude of the elastic modulus in that crystal direction. In the case of an isotropic elastic modulus, this closed surface takes on a perfectly spherical shape. Therefore, the degree of deviation of the 3D representation from a spherical shape reflects the degree of anisotropy in the elastic modulus. In this study, we present the 3D representations of the crystal direction dependence of the linear compressibility (β) and Young's modulus (E) in figures 5 and 6, respectively, as well as their 2D cross-sections in the (ab), (ac), and (bc) planes. It is evident that the closed surfaces representing the crystal direction dependence of both β and E exhibit strong deviations from spherical shape. Similarly, their corresponding cross-sections in the (ab), (ac), and (bc) planes demonstrate significant deviations from circular form, indicating the strong elastic anisotropy of the studied compounds. In all systems analyzed, the maximum values of linear compressibility and Young's modulus (β_{max} and $\mathrm{E_{max}}$) are more than twice the corresponding minimum values (β_{min} and $\mathrm{E_{min}}$).

3.2.3. Sound wave velocities

The knowledge of the velocity of sound waves within a material provides a powerful tool for understanding its physical properties and behavior, and can be applied in numerous fields, ranging from materials science and engineering to medicine and industry. Theoretically, the monocrystalline elastic constants are required for calculating the velocities of the elastic waves propagating in different direction in a medium. The elastic waves velocities can be determined by solving the Christoffel equation [31]:

$$(\mathrm{C_{ijkl}n_j n_k} - \rho \mathrm{V}^2 \delta_{\mathrm{il}})\mathrm{u_l} = 0 \quad (3)$$

In this context, the monocrystalline elastic constant tensor is denoted by $\mathrm{C_{ijkl}}$, with $\vec{n}$ representing the direction of elastic wave propagation, ρ indicating the mass density, $\vec{u}$ representing the direction of elastic wave polarization, and V denoting the wave velocity. The solutions of the Christoffel equation can be classified into two categories: a longitudinal elastic wave, polarized parallel to the propagation direction (V_{L}), and two shear elastic waves ($\mathrm{V_{T1}}$ and $\mathrm{V_{T2}}$), polarized perpendicular to $\vec{n}$.

For tetragonal crystals, the elastic wave velocities that propagate along the [100], [110], and [001] crystal directions can be determined using the following expressions, as detailed in previous literature [32]:

$$V_{L[100]}^{[100]} = \sqrt{\frac{C_{11}}{\rho}};\ V_{T1[010]}^{[100]} = \sqrt{\frac{C_{66}}{\rho}};\ V_{T2[001]}^{[100]} = \sqrt{\frac{C_{66}}{\rho}};$$

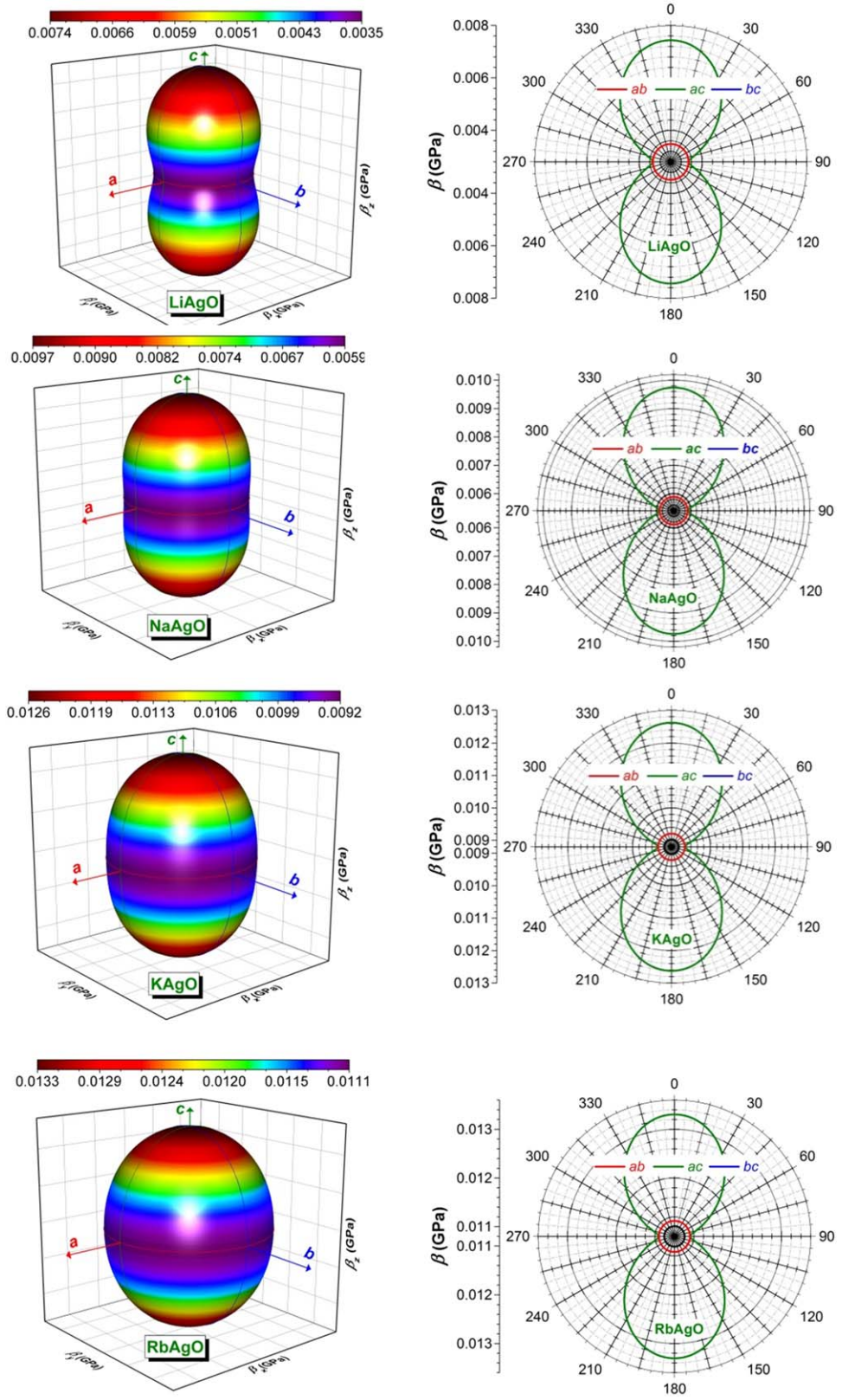

Figure 5. The left panels show representations of the crystal direction dependence of the linear compressibility (β) for LiAgO, NaAgO, KAgO, and RbAgO materials. The right panels depict cross-sections of β in the (ab), (ac), and (bc) planes for these materials.

$$V_{L[110]}^{[110]} = \sqrt{\frac{C_{11} + C_{12} + 2C_{66}}{2\rho}}\,;\; V_{T1[110]}^{[110]} = \sqrt{\frac{C_{11} - C_{12}}{2\rho}}\,;\; V_{T2[100]}^{[110]} = \sqrt{\frac{C_{44}}{2\rho}}$$

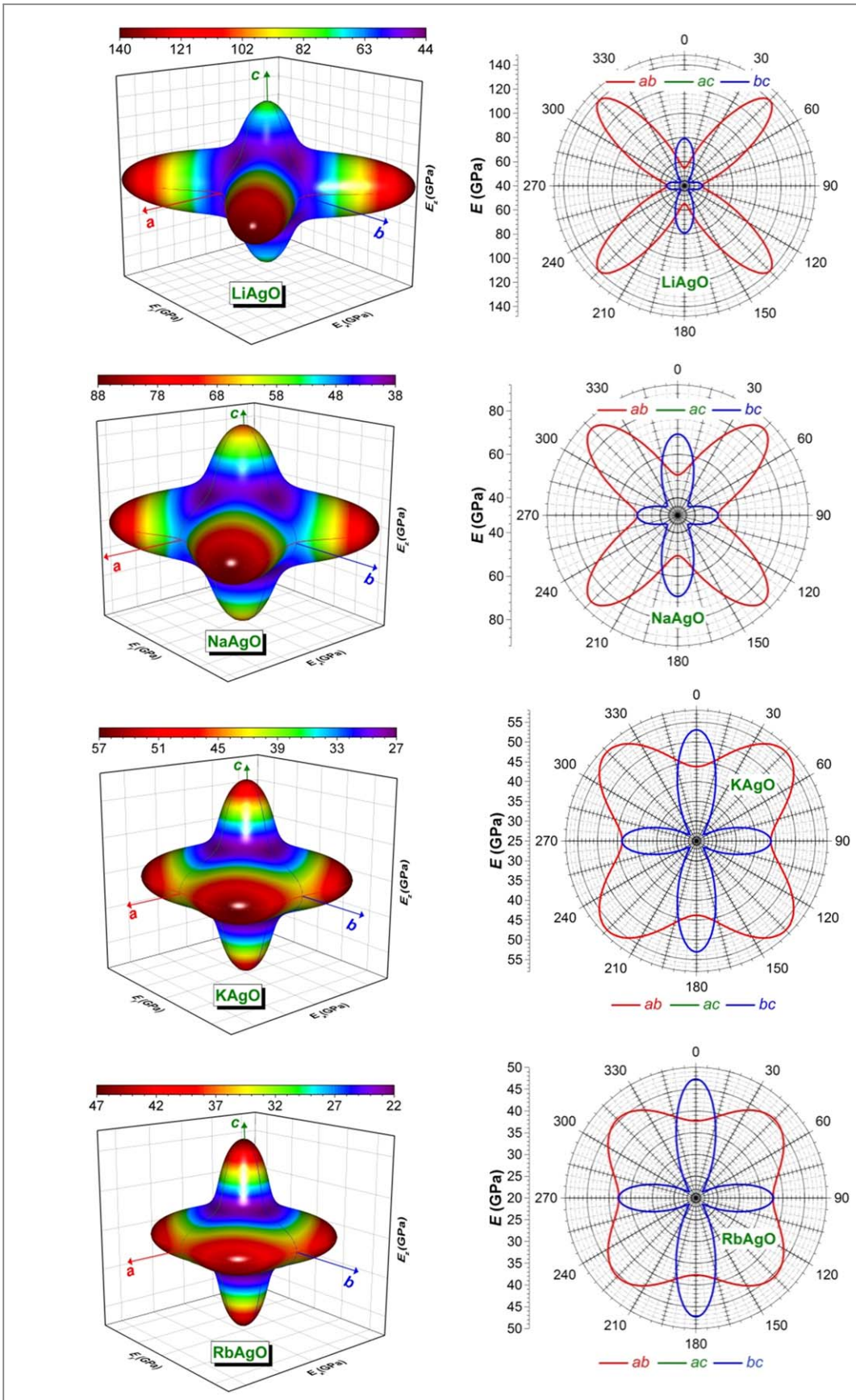

Figure 6. The left panels show representations of the crystal direction dependence of Young's modulus (E) for LiAgO, NaAgO, KAgO, and RbAgO materials. The right panels depict cross-sections of E in the (*ab*), (*ac*), and (*bc*) planes for these materials.

Table 3. Sound velocities (in m/s) calculated from elastic constants for LiAgO, NaAgO, KAgO and RbAgO materials. The velocity of an elastic wave propagating along the $\vec{n}$ direction and polarized along the $\vec{u}$ direction is given by $V^{[\vec{n}]}_{[\vec{u}]}$.

Parameter	Materials			
	LiAgO	NaAgO	KAgO	RbAgO
$V^{[100]}_{L[100]}$	4639.8	4193.8	3756.4	3228.3
$V^{[100]}_{T1[010]}$	3359.8	2708.4	2282.9	1900.0
$V^{[100]}_{T2[001]}$	1712.0	1696.0	1469.5	1221.9
$V^{[110]}_{L[110]}$	5456.7	4641.0	3969.1	3359.6
	1743.6	1839.7	1889.1	1656.8
$V^{[100]}_{T2[001]}$	1712.0	1696.0	1469.5	1221.9
$V^{[001]}_{L[001]}$	4218.6	4026.1	3712.3	3304.6
$V^{[001]}_{T(001)}$	1712.0	1696.0	1469.5	1221.9

$$V^{[001]}_{L[001]} = \sqrt{\frac{C_{33}}{2\rho}};\ V^{[001]}_{T[001]} = \sqrt{\frac{C_{44}}{2\rho}} \tag{4}$$

The numerical estimates of the velocities of the longitudinal and transverse sound waves that propagate along the [100], [110], and [001] crystal directions for XAgO (where X = Li, Na, K, and Rb) are shown in table 3. The findings indicate that longitudinal waves propagate at the fastest and slowest speeds along the [110] and [001] directions, respectively, while transverse waves move at the fastest and slowest speeds along the [110] and [100] directions, respectively. Additionally, the velocities of both longitudinal and transverse elastic waves exhibit a decreasing trend following the order LiAgO, NaAgO, KAgO, and RbAgO. This trend is consistent with the elastic constants C_{ij}s, as the elastic velocities are proportional to the square root of the corresponding elastic constants, as demonstrated in equation (4).

3.2.4. Elastic moduli of the polycrystalline phase

In describing the elasticity of a material composed of multiple crystals, two isotropic elastic moduli are commonly used: the shear modulus (G) and the bulk modulus (B). The isotropic moduli G and B of the polycrystalline phase of a material can theoretically be determined by employing the Voigt-Reuss-Hill approximations to calculate their monocrystalline elastic constants [17–19, 33]. It is worth noting that the Reuss and Voigt approximations provide the extreme limit values of G and B. Hill demonstrated that the effective values of G and B of a polycrystalline material are equivalent to the arithmetic mean of their Reuss and Voigt extremes. Table 2 lists the computed values of the G and B moduli for the materials under study. Additionally, Poisson's ratio (σ) and Young's modulus (E), another pair of interesting elastic moduli, can be determined from G and B [34]. Table 2 provides numerical estimates for σ and E. Based on the results obtained, it can be concluded that:

1. The calculated B values of LiAgO, NaAgO, KAgO, and RbAgO from their monocrystalline elastic constants are in good agreement with the values derived from the Birch equation of state V(P), demonstrating the reliability and accuracy of the calculated elastic constants (tables 1 and 2).
2. The bulk moduli of the studied compounds decrease in the following order: $B^{LiAgO} > B^{NaAgO} > B^{KAgO} > B^{RbAgO}$. This suggests that the average interatomic bond strength decreases from LiAgO to RbAgO, as the bulk modulus represents the resistance to volume change under hydrostatic pressures.
3. The relatively small bulk moduli (less than 100 GPa) of the considered materials indicate their high compressibility. The Young's modulus, which provides information about the stiffness of a material, was calculated to be 68 GPa for LiAgO, 53 GPa for NaAgO, 38 GPa for KAgO, and 31 GPa for RbAgO, indicating a moderate stiffness of these materials.
4. Pugh's empirical criterion [35], which uses the ratio of B to G to determine the brittle or ductile nature of a material, suggests that LiAgO, NaAgO, KAgO, and RbAgO are ductile materials. Ductile materials are machinable and resistant to thermal shocks, and their mechanical properties vary slowly with temperature.
5. The Debye temperature is a key factor in determining the thermal properties of a material and can be estimated from the average sound velocity of an isotropic material, which can be calculated using isotropic G and B [36]. In table 2, we present the longitudinal, transverse, and average sound velocities (V_l, V_t, and V_m,

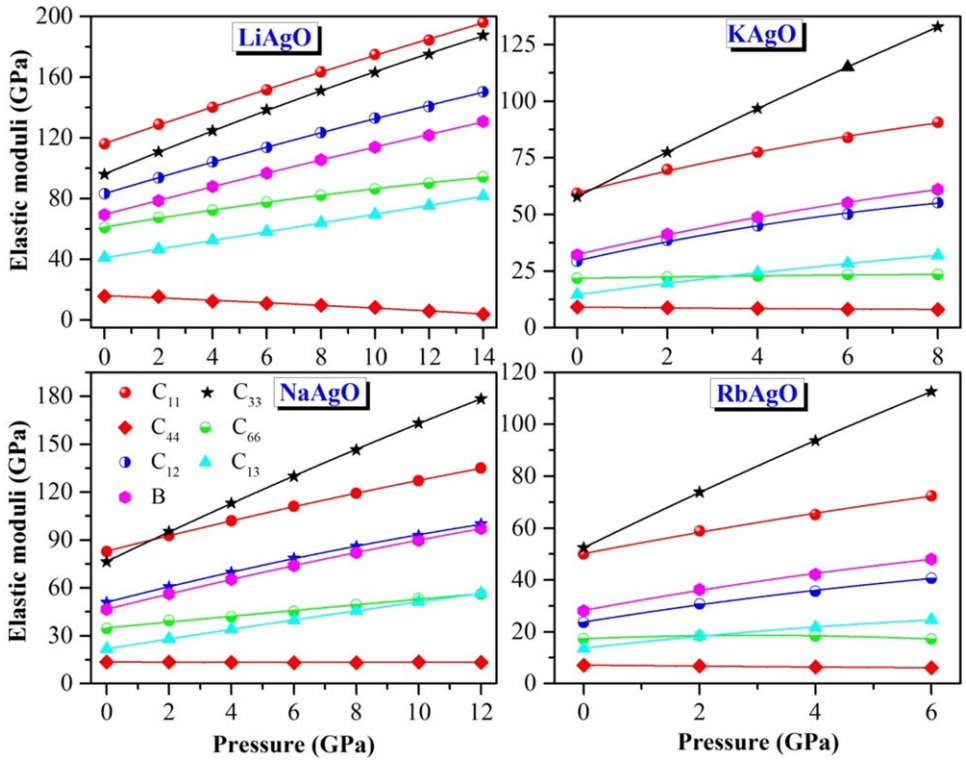

Figure 7. Pressure dependence of the elastic constants C_{ij} and bulk modulus B for LiAgO, NaAgO, KAgO, and RbAgO. The calculated values are shown as symbols, and second-order polynomial fits to the data are shown as continuous lines.

respectively) as well as the Debye temperature (θ_D) for polycrystalline XAgO (X = Li, Na, K, and Rb). As expected, the θ_D values decrease from LiAgO to RbAgO in accordance with the decrease in stiffness.

3.2.5. The effect of pressure on the elastic moduli

The pressure dependence of the independent elastic constants (C_{11}, C_{33}, C_{44}, C_{66}, C_{12} and C_{13}) and the bulk modulus (B) of the investigated materials are illustrated in figure 7. It should be noted that the computed C_{ij}(P) values were determined specifically for pressure ranges that align with the established mechanical stability limits of the compound [37, 38]: $(\tilde{C}_{11} - \tilde{C}_{12}) > 0$; $(\tilde{C}_{11} + \tilde{C}_{33} + 2\tilde{C}_{13}) > 0$; $\tilde{C}_{ii} > 0$; $(2\tilde{C}_{11} + \tilde{C}_{33} + 2\tilde{C}_{12} + 4\tilde{C}_{13}) > 0$; where $\tilde{C}_{ii} = C_{ii} - P$; (I = 1, 3, 4, 6); $\tilde{C}_{12} = C_{12} - P$; $\tilde{C}_{13} = C_{13} - P$.The symbols in the figure represent the calculated values of the elastic constants (C_{ij}) and bulk modulus (B) at different pressures, while the solid lines represent the fits of B(P) and C_{ij}(P) to the second-order polynomials given in table 4. Our analysis indicates that the elastic constants C_{11}, C_{33}, C_{66}, C_{12} and C_{13} increase as the pressure is increased. Nonetheless, a discernible trend is observed in the behavior of C_{44} as pressure increases, indicating a gradual decline. This observation implies that these materials could potentially demonstrate mechanical instability under elevated pressures that surpass the predefined thresholds of mechanical stability [4], thus leading to a scenario where the conditions for mechanical stability [37, 38] are no longer met. The obtained values for the shear modulus C_{44} suggest that the mechanical stability criteria could be satisfied approximately in the pressure ranges of 0 to 15 GPa for LiAgO, 0 to 13 GPa for NaAgO, 0 to 9 GPa for KAgO, and 0 to 7 GPa for RbAgO.

3.3. Thermodynamic properties

Knowledge of the thermodynamic properties of materials is essential for designing, optimizing, and developing materials for a wide range of applications. The study of thermodynamics provides a fundamental understanding of how materials behave under different conditions, and this knowledge is essential for advancing technology and addressing global challenges.The quasi-harmonic Debye model, as implemented in the Gibbs program [21], was utilized to investigate the thermodynamic properties of LiAgO, NaAgO, KAgO, and RbAgO materials.

Figure 8 illustrates the normalized-volume versus temperature variation at various fixed pressures of 0, 3 and 6 GPa for the aforementioned materials. It is generally observed that the normalized-volume increases with increasing temperature for a given pressure, indicating the increase of compressibility of the compounds due to the temperature increase.Note that the rate of volume increase with temperature decreases with increasing pressure for all materials except KAgO. Moreover, as the temperature increases, the normalized volume V/V_0

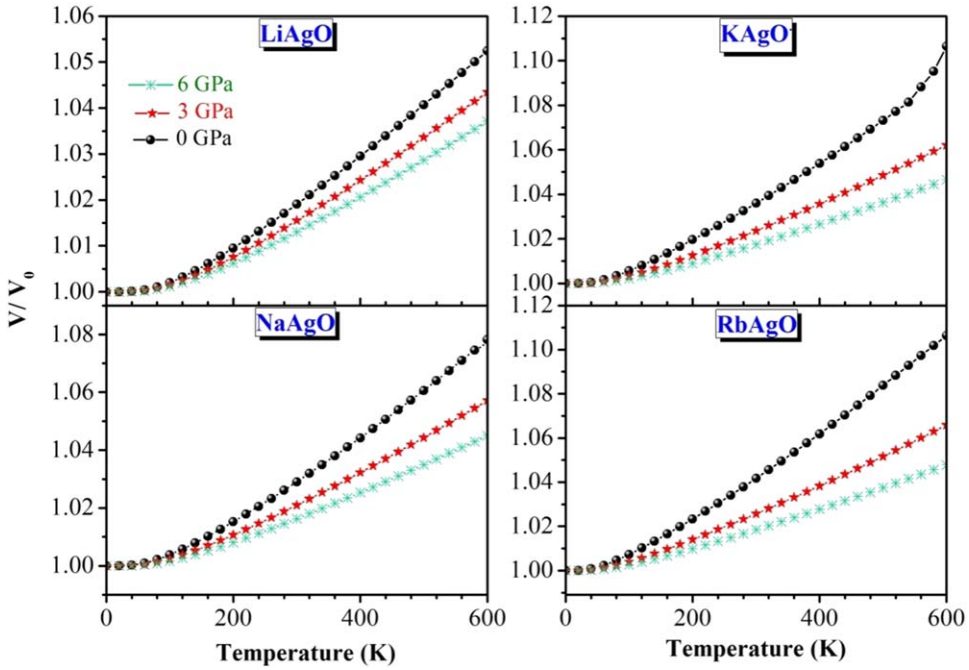

Figure 8. The normalized unit cell volume (V/V_0) changes as a function of temperature at different fixed pressures for the LiAgO, NaAgO, KAgO, and RbAgO materials.

Table 4. The quadratic polynomials describing the dependence of the elastic constants on the pressure of the compounds LiAgO, NaAgO, KAgO and RbAgO. The fitting was performed on the *ab initio* calculated C_{ij}s at discrete pressures.The pressure, P, is given in GPa.

System	Elastic constants (GPa)
LiAgO	$C_{11} = 116.31 + 6.12 \times P - 0.0330 \times P^2$
	$C_{33} = 96.32 + 7.32 \times P - 0.0590 \times P^2$
	$C_{44} = 16.10 - 0.72 \times P - 0.0098 \times P^2$
	$C_{66} = 61.22 + 2.98 \times P - 0.0462 \times P^2$
	$C_{12} = 83.30 + 5.33 \times P - 0.0406 \times P^2$
	$C_{13} = 41.08 + 2.80 \times P + 0.0056 \times P^2$
	$B = 69.53 + 4.66 \times P - 0.0229 \times P^2$
NaAgO	$C_{11} = 83.01 + 4.95 \times P - 0.0527 \times P^2$
	$C_{33} = 76.58 + 9.36 \times P - 0.0732 \times P^2$
	$C_{44} = 13.61 - 0.084 \times P + 0.0065 \times P^2$
	$C_{66} = 34.94 + 1.84 \times P - 0.0050 \times P^2$
	$C_{12} = 51.01 + 5.03 \times P - 0.0807 \times P^2$
	$C_{13} = 21.77 + 3.14 \times P - 0.0203 \times P^2$
	$B = 46.58 + 4.91 \times P - 0.0586 \times P^2$
KAgO	$C_{11} = 59.57 + 5.11 \times P - 0.1583 \times P^2$
	$C_{33} = 57.85 + 10.04 \times P - 0.0839 \times P^2$
	$C_{44} = 9.08 - 0.19 \times P + 0.0081 \times P^2$
	$C_{66} = 21.82 + 0.31 \times P - 0.0121 \times P^2$
	$C_{12} = 29.56 + 5.03 \times P - 0.0807 \times P^2$
	$C_{13} = 14.58 + 2.63 \times P - 0.0581 \times P^2$
	$B = 32.31 + 4.60 \times P - 0.1281 \times P^2$
RbAgO	$C_{11} = 50.13 + 4.30 \times P - 0.1025 \times P^2$
	$C_{33} = 52.39 + 10.97 \times P - 0.1575 \times P^2$
	$C_{44} = 7.16 - 0.2035 \times P + 0.0054 \times P^2$
	$C_{66} = 17.32 + 0.86 \times P - 0.1480 \times P^2$
	$C_{12} = 23.78 + 3.56 \times P - 0.1292 \times P^2$
	$C_{13} = 13.67 + 2.52 \times P - 0.1187 \times P^2$
	$B = 28.23 + 4.16 \times P - 0.1465 \times P^2$

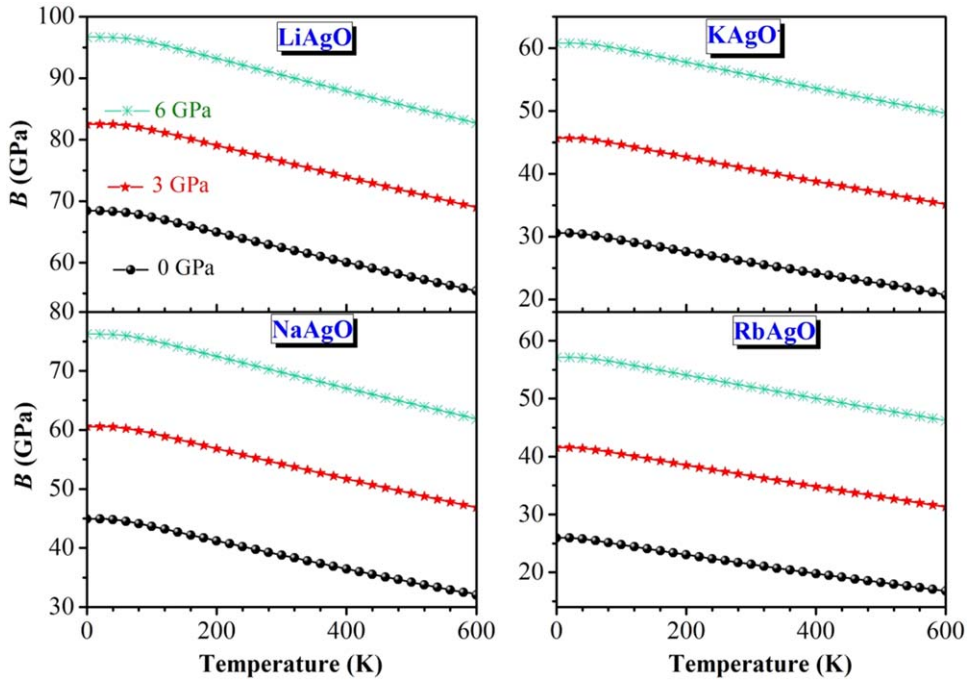

Figure 9. The temperature-dependent behavior of the bulk modulus for LiAgO, NaAgO, KAgO, and RbAgO materials under various pressures. The results demonstrate a negative correlation between the bulk modulus and temperature, whereas a positive relationship is observed between the bulk modulus and pressure for all materials.

decreases more rapidly with increasing pressure due to the increase of compressibility with increasing temperature. The unit cell volume values were calculated to be 278.25Å^3 for LiAgO, 358.41Å^3 for NaAgO, 446.20Å^3 for KAgO, and 502.25Å^3 for RbAgO at zero pressure and room temperature (0 GPa and 300 K).

Figure 9 depicts the variations in the bulk modulus (B) of LiAgO, NaAgO, KAgO, and RbAgO materials as a function of temperatureat fixed pressures of 0, 3 and 6 GPa. The results demonstrate that the bulk modulus remains relatively constant for temperatures below 100 K and then decreases linearly with increasing temperature. The bulk modulus increases with increasing pressure. At room temperature (300 K) and zero pressure, the bulk modulus values for LiAgO, NaAgO, KAgO, and RbAgO are approximately 66 GPa, 44 GPa, 34 GPa, and 31 GPa, respectively.

Figure 10 depicts the calculated temperature-dependent volume thermal expansion coefficient (α) for LiAgO, NaAgO, KAgO, and RbAgO materials at various fixed pressuresof 0, 3 and 6 GPa. The findings indicate that α experiences a sharp upsurge with increasing temperature in the range of 0–200 K at a fixed pressure, particularly at zero pressure. However, for temperatures exceeding 200 K, the trend of α elevation becomes less significant and ultimately tends to a linear growth. Note that for $T > 200\ K$, α increases sluggishly and practically stabilizes at pressures of 5 and 10 GPa in KAgO and RbAgO. This implies that the temperatures impact on α under high pressure is quite weak for these substances.Moreover, α coefficient diminishes significantly as pressure rises. At zero pressure and room temperature (300 K), the α coefficient is approximately equal to $8.17 \times 10^{-5}K^{-1}$, $9.73 \times 10^{-5}K^{-1}$, $2.14 \times 10^{-5}K^{-1}$, and $2.87 \times 10^{-5}K^{-1}$ for LiAgO, NaAgO,KAgO, and RbAgO, respectively.

Figures 11 and 12 display the curves illustrating the relationship between constant volume heat capacity (C_V) and constant pressure heat capacity (C_P) with temperature at fixed pressures of 0, 3 and 6 GPa. According to the Debye model, the results demonstrate that C_V and C_P are proportional to T^3 at low temperatures. At ambient temperature (300 K) and zero pressure, the values of C_V (C_P) are approximately 278 J.mol^{-1}.K^{-1} (291 J.mol^{-1}.K^{-1}) for LiAgO, 285 J.mol^{-1}.K^{-1} (301 J.mol^{-1}.K^{-1}) for NaAgO, 288 J.mol^{-1}.K^{-1} (318 J.mol^{-1}.K^{-1}) for KAgO and 291 J.mol^{-1}.K^{-1} (315 J.mol^{-1}.K^{-1}) for RbAgO. Nevertheless, as temperature rises, C_V approaches the Dulong-Petit limit (roughly equal to 300 J.mol^{-1}.K^{-1}), while C_P tends to increase linearly. Increasing pressure leads to a reduction in both C_V and C_P values at a fixed temperature. However, the impact of temperature on C_P is more significant than that of pressure.

Figure 13 illustrates the relationship between the Debye temperature (θ_D) -a crucial thermodynamic parameter that correlates with several physical properties of solids, including melting temperatures, elastic constants, and specific heat- and temperature at fixed pressures of 0, 3 and 6 GPa. It was observed that θ_D remains relatively constant in the temperature range of 0–100 K for all studied materials. For temperatures

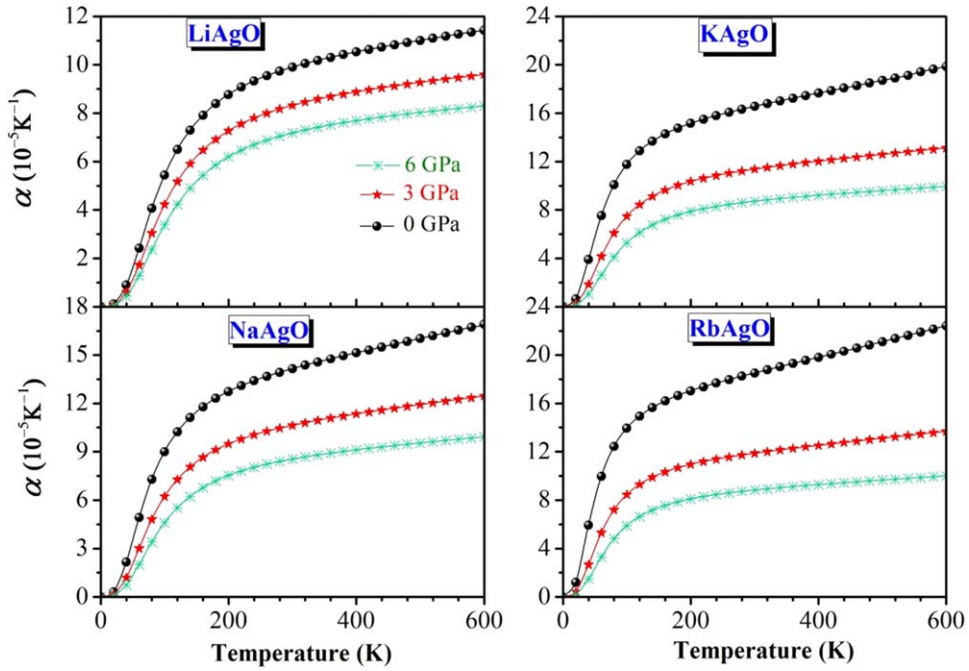

Figure 10. Temperature dependence of the volume thermal expansion coefficient for LiAgO, NaAgO, KAgO and RbAgO at various fixed pressure values.

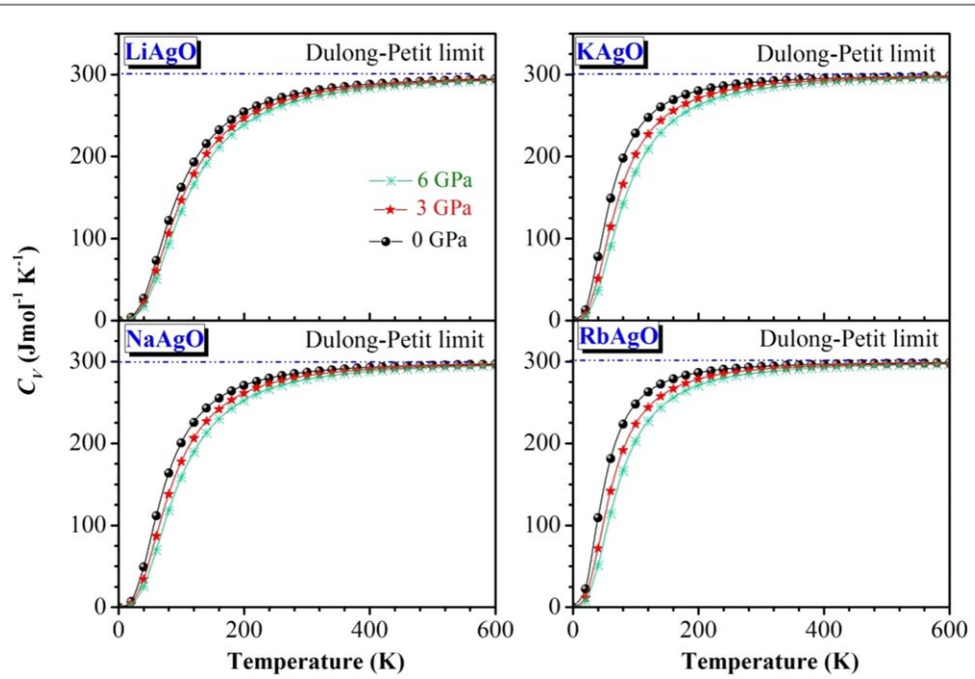

Figure 11. Temperature dependence of the constant volume heat capacity (C_V) for LiAgO, NaAgO, KAgO and RbAgO at various fixed pressures.

above 100 K, $\theta_D$decreases with increasing temperature. This decrease is significant for LiAgO and NaAgO, and its propensity decreases with increasing pressure. At ambient temperature (300 K) and zero pressure, the computed value of $\theta_D$is 369 K for LiAgO, 299 K for NaAgO, 267 K for KAgO, and 227 K for RbAgO. The yielded values of θ_D by the quasi-harmonic Debye approximation are in excellent agreement with the corresponding values obtained from the elastic constants (340 K for LiAgO, 288 K for NaAgO, 275 K for KAgO, and 210 K for RbAgO). This agreement suggests that the quasi-harmonic approximation provides a viable alternative for accounting for thermal effects without the need for computationally demanding procedures.

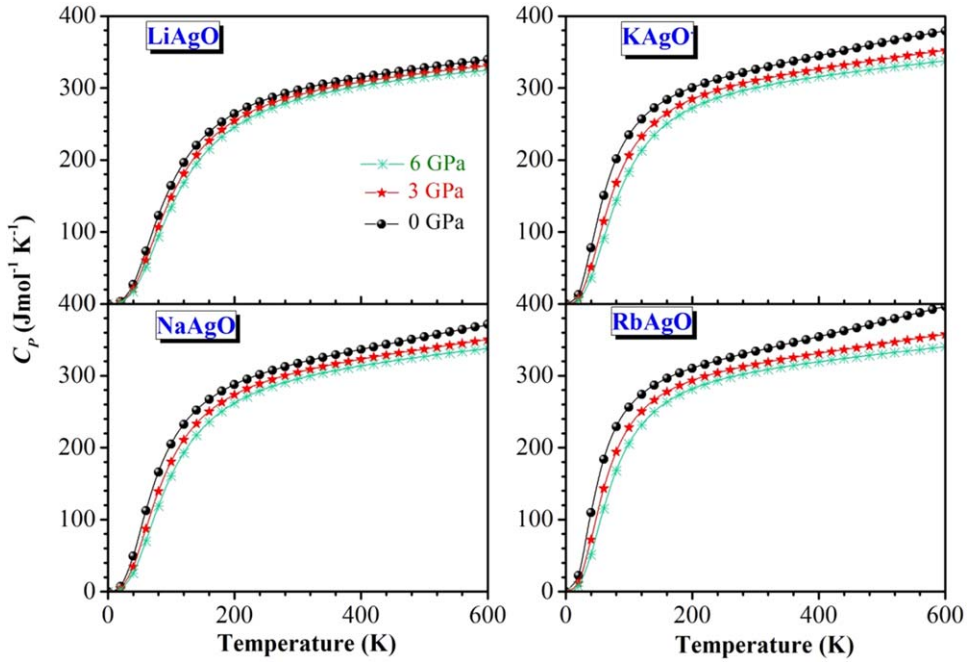

Figure 12. Temperature dependence of the constant pressure heat capacity (C_P) for LiAgO, NaAgO, KAgO and RbAgO at various fixed pressures.

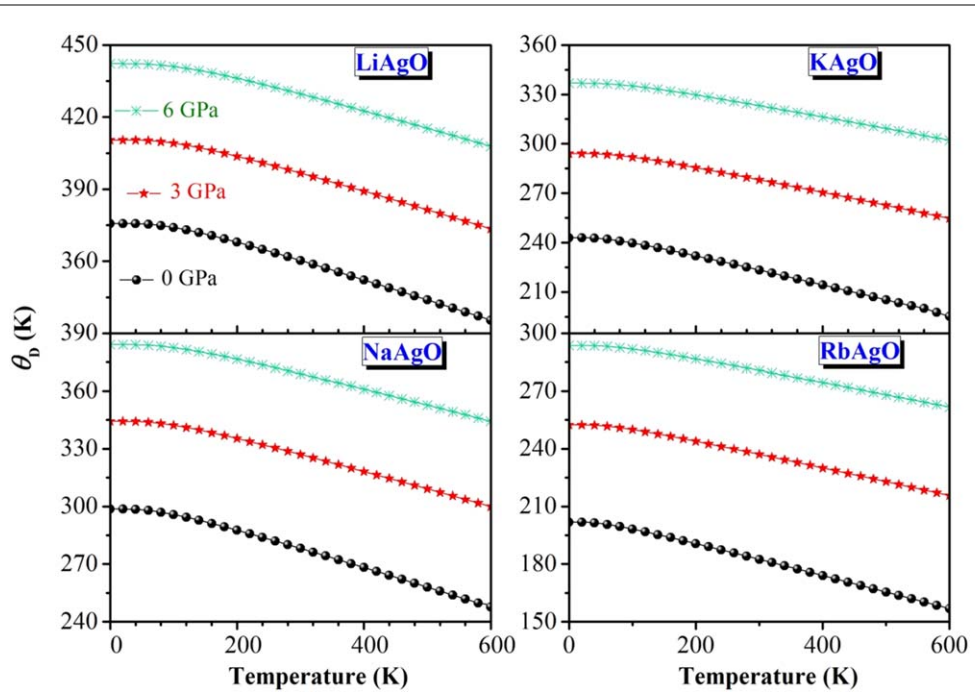

Figure 13. Temperature dependence of the Debye temperature for LiAgO, NaAgO, KAgO and RbAgO at various fixed pressures.

4. Conclusions

In this investigation, we employed *ab initio* pseudopotential plane wave calculations to analyze the structural, elastic, and thermodynamic properties of XAgO (X = Li, Na, K, and Rb) oxides. The results exhibit anexcellent agreement between the optimized lattice parameters and reported experimental data, and a pressure-dependent anisotropic behavior of the lattice constants. All the examined materials are found to be mechanically stable at zero pressure with significant elastic anisotropy. By utilizing the calculated elastic constants, we identified the sound wave propagation velocities along specific crystallographic directions. Monocrystalline elastic constants and polycrystalline elastic moduli exhibit a decreasing trend as X varies from Li to Rb, suggesting a reduction in

stiffness. According to Pugh's criterion, all considered materials demonstrate ductile behavior. The pressure dependence of the elastic constants of the title compounds reveals that they remain mechanically stable under pressure up to approximately 15 GPa for LiAgO, 13 GPa for NaAgO, 9 GPa for KAgO, and 7 GPa for RbAgO. It is noteworthy that the elastic constants increase with increasing pressure for all four compounds, except for the shear modulus C_{44}, which decreases with increasing pressure. This suggests that the title compounds may become mechanically unstable outside the aforementioned pressure intervals, as the shear modulus is a measure of a materials resistance to shear deformation. We also investigated the temperature dependence of bulk modulus, unit cell volume, heat capacities, volume thermal expansion coefficient, and Debye temperature in the range of 0–600 K at fixed pressures of 0, 3 and 6 GPa using the quasi-harmonic Debye approximation. Our results demonstrate that higher temperatures led to a lower bulk modulus, higher heat capacities, and greater volume expansion coefficient at a given pressure, whereas higher pressures induce the opposite effects. The volume thermal expansion coefficient and heat capacity tend to remain stable at high pressures and temperatures.

Acknowledgment

The author S Bin Omran acknowledges the Researchers Supporting Project number (RSP2023R82), King Saud University, Riyadh, Saudi Arabia.

Data availability statement

The data cannot be made publicly available upon publication because no suitable repository exists for hosting data in this field of study. The data that support the findings of this study are available upon reasonable request from the authors.

ORCID iDs

Djamel Allali https://orcid.org/0000-0001-9680-7340
Saber Saad Essaoud https://orcid.org/0000-0002-6337-3184
Missoum Radjai https://orcid.org/0000-0002-0313-7155
Rabah Khenata https://orcid.org/0000-0002-5573-1711
Yarub Al-Douri https://orcid.org/0000-0002-5175-6372

References

[1] Halasyamani P S and Poeppelmeier K R 1998 Noncentrosymmetric oxides *Chem. Mater.* **10** 2753–69
[2] Chung J Y, Yeon S, Ryu H, You T-S, Jang J I and Ok K M 2022 Nonlinear optical properties of a new polar bismuth tellurium oxide fluoride, $Bi_3F(TeO_3)(TeO_2F_2)_3$ *J. Alloys Compd.* **895** 162603
[3] Bouhemadou A, Allali D, Boudiaf K, Al Qarni B, Bin-Omran S, Khenata R and Al-Douri Y 2019 Electronic, optical, elastic, thermoelectric and thermodynamic properties of the spinel oxides $ZnRh_2O_4$ and $CdRh_2O_4$ *J. Alloys Compd.* **774** 299–314
[4] Umamaheswari R, Yogeswari M and Kalpana G 2013 Electronic properties and structural phase transition in A_4 [M_4O_4] (A = Li, Na, K and Rb; M = Ag and Cu): A first principles study *Solid State Commun.* **155** 62–8
[5] Klassen H and Hoppe R 1982 Die $K_4[Ag_4O_4]$—strukturfamilie *Z. Anorg. Allg. Chem.* **485** 101–14
[6] Losert W and Hoppe R 1985 Zur Kenntnis der $K_4[Ag_4O_4]$-Verwandtschaft *Z. Anorg. Allg. Chem.* **524** 7–16
[7] Fischer D, Carl W, Glaum H and Hoppe R 1990 Zur Struktur der KAgO-Verwandtschaft Neubestimmung an AAgO = $A_4[Ag_4O_4]$ (A = Na–Rb) mit einer Bemerkung zu CsCuO (und neue Rechnungen an $A_4[M_4O_4,]$ A = Li−Rb für M = Cu bzw. A = Cs für M = Ag) *Z. Anorg. Allg. Chem.* **585** 75–81
[8] Verma P, Singh C, Kamlesh P K, Kaur K and Verma A S 2023 Nowotny-Juza phase KBeX (X = N, P, As, Sb, and Bi) half-Heusler compounds: applicability in photovoltaics and thermoelectric generators *J. Mol. Model.* **29** 23–36
[9] Kamlesh P K, Agrawal R, Rani U and Verma A S 2022 Comprehensive ab-initio calculations of AlNiX (X = P, As and Sb) half-Heusler compounds: stabilities and applications as green energy resources *Mater. Chem. Phys.* **275** 125233–49
[10] Clark S J, Segall M D, Pickard C J, Hasnip P J, Probert M I, Refson K and Payne M C J Zf K-C M 2005 *First principles methods using CASTEP* **220** 567–70
[11] Perdew J P, Ruzsinszky A, Csonka G I, Vydrov O A, Scuseria G E, Constantin L A, Zhou X and Burke K 2008 Restoring the density-gradient expansionfor exchange in solids and surfaces *Phys. Rev. Lett.* **100** 136406–1
[12] Wu Z and Cohen R E 2006 More accurate generalized gradient approximation for solids *Physical Review B* **73** 235116
[13] Vanderbilt D 1990 Soft self-consistent pseudopotentials in a generalized eigenvalue formalism *Physical Review B* **41** 7892–5
[14] Monkhorst H J and Pack J D 1976 Special points for Brillouin-zone integrations *Physical Review B* **13** 5188–92
[15] Fischer T H and Almlof J 1992 General methods for geometry and wave function optimization *J. Phys. Chem.* **96** 9768–74
[16] Milman V and Warren M C 2000 Elasticity of hexagonal BeO *J. Phys. Condens. Matter* **13** 241–51
[17] Reuss A 1929 Berechnung der Fließgrenze von Mischkristallen auf Grund der Plastizitätsbedingung für Einkristalle *ZAMM - Journal of Applied Mathematics and Mechanics/Zeitschrift für Angewandte Mathematik und Mechanik* **9** 49–58
[18] Voigt W 1928 Lehrbuch der Kristallphysik *Teubner, Leipzig*u.a

[19] Hill R 1952 The elastic behaviour of a crystalline aggregate *Proc. Phys. Soc. London, Sect. A* **65** 349–54
[20] Hill R 1963 Elastic properties of reinforced solids: Some theoretical principles *J. Mech. Phys. Solids* **11** 357–72
[21] Blanco M A, Francisco E and Luaña V 2004 GIBBS: isothermal-isobaric thermodynamics of solids from energy curves using a quasi-harmonic Debye model *Comput. Phys. Commun.* **158** 57–72
[22] Khuili M, Bounbaa M, Fazouan N, Abou Elmakarim H, Sadiki Y, S.Al-Qaisi K and Maher 2023 First-principles study of structural, elastic, optoelectronic and thermoelectric properties of B-site-ordered quadruple perovskite $Ba_4Bi_3NaO_{12}$ *J. Solid State Chem.* **322** 123955
[23] Birch F 1978 Finite strain isotherm and velocities for single-crystal and polycrystalline NaCl at high pressures and 300 K *Journal of Geophysical Research: Solid Earth* **83** 1257–68
[24] Birch F 1947 Finite elastic strain of cubic crystals *Phys. Rev.* **71** 809
[25] Bouhemadou A, Boudrifa O, Guechi N, Khenata R, Al-Douri Y, Uğur Ş, Ghebouli B and Bin-Omran S 2014 Structural, elastic, electronic, chemical bonding and optical properties of Cu-based oxides ACuO (A = Li, Na, K and Rb): an *ab initio* study *Comput. Mater. Sci.* **81** 561–74
[26] Bedjaoui A, Bouhemadou A and Bin-Omran S 2016 Structural, elastic and thermodynamic properties of tetragonal and orthorhombic polymorphs of Sr_2GeN_2: an *ab initio* investigation *High Pressure Res.* **36** 198–219
[27] Reffas M, Bouhemadou A, Haddadi K, Bin-Omran S and Louail L 2014 '*Ab initio* prediction of the structural, electronic, elastic and thermodynamic properties of the tetragonal ternary intermetallics XCu_2Si_2 (X = Ca, Sr) *The European Physical Journal B* **87** 283
[28] Khireddine A, Bouhemadou A, Alnujaim S, Guechi N, Bin-Omran S, Al-Douri Y, Khenata R, Maabed S and Kushwaha A K 2021 'First-principles predictions of the structural, electronic, optical and elastic properties of the zintl-phases AE3GaAs3 (AE = Sr, Ba) *Solid State Sci.* **114** 106563
[29] Gherriche A, Bouhemadou A, Al-Douri Y, Bin-Omran S, Khenata R and Hadi M A 2021 *Ab initio* exploration of the structural, elastic, electronic and optical properties of a new layered perovskite-type oxyfluoride: $CsSrNb_2O_6F$ *Mater. Sci. Semicond. Process.* **131** 105890
[30] Nye J F 2012 Physical properties of crystals : their representation by tensors and matrices
[31] Landau L D L E M 2008 *Theory of elasticity* (Butterworth-Heinemann)
[32] Royer D D E 2000 *Elastic waves in solids I+II* (Berlin: Springer)
[33] Mehl M J, Klein B M and Papaconstantopoulos D A J P 1995 *Intermetallic compounds: principle and practice* **1** 195–210
[34] Pugh S F 1954 XCII. Relations between the elastic moduli and the plastic properties of polycrystalline pure metals *The London, Edinburgh, and Dublin Philosophical Magazine and Journal of Science* **45** 823–43
[35] Cazzani A and Rovati M 2005 Extrema of Young's modulus for elastic solids with tetragonal symmetry *Int. J. Solids Struct.* **42** 5057–96
[36] Bouhemadou A 2008 Prediction study of structural and elastic properties under pressure effect of M2SnC (M = Ti, Zr, Nb, Hf) *Physica B* **403** 2707–13
[37] Wu Z J, Zhao E J, Xiang H P, Hao X F, Liu X J and Meng J 2007 Crystal structures and elastic properties of superhard Ir N2 and Ir N3 from first principles *Physical Review B* **76** 054115
[38] Sin'Ko G V and Smirnov N A 2002 *Ab initio* calculations of elastic constants and thermodynamic properties of bcc, fcc, and hcp Al crystals under pressure *J. Phys. Condens. Matter* **14** 6989